JCTC Journal of Chemical Theory and Computation

Effects of the Aluminum Content of a Zeolite Framework: A DFT/MM Hybrid Approach Based on Cluster Models Embedded in an Elastic Polarizable Environment

Elena A. Ivanova Shor,[†] Alexei M. Shor,[†] Vladimir A. Nasluzov,*[,†] Georgi N. Vayssilov,*[,‡] and Notker Rösch*[,§]

Institute of Chemistry and Chemical Technology, Russian Academy of Sciences, 660049 Krasnoyarsk, Russian Federation, Faculty of Chemistry, University of Sofia, 1126 Sofia, Bulgaria, and Department Chemie, Technische Universität München, 85747 Garching, Germany

Received October 26, 2004

Abstract: We report the first computational study with a sophisticated quantum mechanics/molecular mechanics (QM/MM) technique that addresses the effect of the aluminum content on the properties of acidic zeolites. To account for both electrostatic and mechanical interaction between the QM cluster and its MM environment, we used cluster models embedded in the covalent variant of the elastic polarizable environment (covEPE) [Nasluzov, V. A.; Ivanova, E. A.; Shor, A. M.; Vayssilov, G. N.; Birkenheuer, U.; Rösch, N. *J. Phys. Chem. B* **2003**, *107*, 2228]. For the practical application of the covEPE method, it was necessary to develop a new force field for Al containing zeolites. Two types of zeolite materials, FAU and MFI, were employed as examples. We modeled the variation of the Al content both in the MM environment and in the QM cluster, and we studied pertinent properties of bridging OH groups of the zeolite frameworks, OH vibrational frequencies, and deprotonation energies. The computational results suggest that the local structure and the location of the OH groups exert a stronger effect than the variation of the Al content of the framework.

1. Introduction

The contribution of computational methods for investigating structure and catalytic properties of zeolite materials is nowadays commonly acknowledged.[1] Still, large unit cells of realistic zeolite systems present a major obstacle that restricts the wide-spread application of simulation methods. Ab initio calculations that account for the periodicity of such systems are, as a rule, computationally expensive and, therefore, available mainly for highly symmetric frameworks with unit cell of modest size.[2,3] The symmetry of practically important zeolite systems is often lowered by the presence of defects (e.g. interstitials or adsorbed molecules) which further complicate calculations. A well-recognized approach for studying such local phenomena employs cluster models where active sites are represented by a chemically relevant finite part of the lattice.[4−7] A significant drawback of this approach is that it totally neglects the influence of the surrounding crystal lattice on the reaction center. Therefore, such models are not suitable for a variety of pertinent problems of zeolite chemistry where one has to discriminate active sites in structurally or chemically different environments, e.g. Brønsted acidic sites in aluminosilicates of different framework structures and varying Al content.

Hybrid quantum mechanics/molecular mechanics (QM/MM) methods[8,9] are known to afford an accurate treatment of such problems by taking into account thousands of atoms

* Corresponding authors e-mail: nv@krsk.info (V.A.N.), gnv@chem.uni-sofia.bg (G.N.V.), roesch@ch.tum.de (N.R.).
[†] Russian Academy of Sciences.
[‡] University of Sofia.
[§] Technische Universität München.

10.1021/ct049910n CCC: $30.25
Published on Web 04/19/2005

in the system at the cost of dozens. This efficiency is achieved by describing only the immediate neighborhood of the active site (cluster) with a high precision QM method and by representing its environment at an more economic level, e.g. with a MM method. Such QM/MM schemes inherit the capability to model easily point defects (including charged ones) from strategies based on traditional (isolated) cluster models but overcome their deficiencies connected with neglecting steric constraints and the electrostatic field of the environment. However, to properly construct a QM/MM method, one has to account both for long-range electrostatic effects of the environment and the mechanical coupling of the QM cluster with its immediate surrounding. In addition, it is highly desirable to preserve the variationality of the method as well as to reduce and control the influence of the QM/MM border region.

A specific complication of high-level, accurate QM/MM schemes is connected with the requirement to use a properly parametrized MM force field (FF) for describing both mechanical and electrostatic interactions between the QM region and its MM environment. In view of the polar covalent nature of siliceous and zeolite materials, it is crucial to model correctly the electrostatic properties of the framework. A practical and efficient way to achieve this goal assigns so-called potential derived point charges (PDC)[10] to lattice centers and represents the polarizability of lattice oxygen centers by a "shell model" scheme.[11] However, to the best of our knowledge, so far no force field has been developed for Al-containing zeolites that simultaneously uses such charges and allows for the polarization of O centers. The PDC-based rigid ion model of Blake et al.[12] is applicable to Na-forms of aluminosilicates only, whereas the model of van Santen et al.[13] for H-forms of aluminoslicates relies on a rigid-ion parametrization with atomic charges that are relatively large compared to those derived from the electrostatic potential. The valence force field of Hill and Sauer[14] utilizes rather small charges; at the other extreme, shell models[15,16] employ too large (absolute) formal charges. These force fields aim at reproducing structural features of zeolites rather than their electrostatic field. Indeed, the latter parametrizations[16] are invoked in the QM-Pot cluster embedding which, at the quantum mechanical level, neglects long-range interactions across the QM/MM border.[9] Available PDC-based force fields for siliceous frameworks[12,17] are also limited in number and scope; in particular, when used in embedded cluster schemes, they are suitable for modeling pure silica systems or systems with an extremely low Al content where it is sufficient to locate Al atoms only in the QM part of the system.[8,17]

The present work is the first QM/MM study of the Al content effect on the properties of Brønsted active centers in zeolites at the level of a combined electrostatic and mechanical embedding. We used our covEPE embedding scheme[17] but developed a new FF for Al containing zeolites that provides both a shell model treatment of oxygen centers and assigns PDC to all centers of the zeolite framework, including protons of bridging OH groups. This FF is an extension of our previously reported PDC-based shell model FF for pure siliceous materials.[17] With these tools, we investigated to which degree the structure, OH frequencies, and deprotonation energies of Brønsted acidic sites in zeolites are affected by changes of its Al loading. Our goal was to derive a general correlation between chemical composition and properties of the zeolite.

We studied a faujasite (FAU) zeolite with a wide range of Si/Al ratios (∞, 47, 23, 11). Such highly dealuminated lattices are not quite typical for faujasite, the Si/Al ratio of which is usually below 3.[18,19] To model structures with high local Al concentration, we considered two interacting (or "paired") acidic sites, i.e., a situation where Al centers are located at closest possible distance. We compared the effects of the Al content with that of the local structure around the acidic OH group in a regular framework. For that purpose, we modeled Brønsted centers located at O1(H) and O3(H) crystallographic positions of a faujasite lattice as well as at Al7−O17(H)−Si4 sites of zeolite HZSM-5 (with MFI structure). Moreover, we discussed the accuracy of our results with regard to size limitations of QM cluster models as well as to the proximity of active Brønsted centers and the QM/MM boundary.

2. Method and Models

2.1. CovEPE Embedding Approach. The covEPE embedding scheme[17] is specially set up to deal with systems that feature covalent bonding. Dangling bonds of the model QM cluster are saturated with monovalent atomic pseudopotentials (*pp*) representing crystal lattice oxygen centers. The parameters of these border atoms are adjusted to mimic the behavior of real oxygen atoms as well as to minimize the perturbation of the electrostatic field at the cluster boundary. The method completely and explicitly includes both mechanical and electrostatic interactions between the QM cluster and its MM lattice (*lat*) environment. For a correct description of the cluster surrounding, a force field is required that is based on potential-derived charges and accounts for the polarization of lattice centers.

The entire system under study is divided into an active area, region I, treated at the QM level, and its MM surrounding, region II, described with a force field. region II is further partitioned into areas of explicit optimization (IIa), with Mott-Littleton polarization (IIb), and an external area (IIc). The total energy E_{tot} of the QM/MM system comprises three contributions which describe the interactions in the QM cluster, E_{cl}, and the coupling between the QM cluster and its environment, E_{int}, as well as the interactions within the MM lattice, E_{lat}.[17]

The environment affects the QM cluster via its Madelung field and short-range forces. The last contribution includes the FF interaction between regions I and IIa as well as forces acting on the QM/MM boundary to restore the structure of the frontier region of the cluster model as in a defect-free lattice. The environmental lattice is subjected to a displacement polarization, and the oxygen atoms of the MM framework are also allowed to be polarized in shell-model fashion due to changes of the charge distribution in the QM cluster.

A covEPE treatment consists of the following steps: (i) optimization of the structure of the ideal (regular − *reg*)

periodic lattice with an atomistic force field; (ii) optimization of the QM cluster (*cl*) modeling region I as *reference* (*ref*) embedded in a "frozen" environment; (iii) energy minimization of the *defect* site under study (e.g. an adsorption complex or defect center) created within the QM part; and (iv) the relaxation of region II while accounting for Coulomb and short-range coupling with region I. The structure of the whole system, comprising QM and classical regions, is determined variationally by minimizing the total energy in steps (iii) and (iv). One may expect artificial changes of structure and charge distribution of an embedded system relative to the system treated completely classically—even without any guest species, impurities, or defects. To eliminate these artifacts caused by the mismatch of descriptions inherent to any hybrid method, one applies correction terms to the charge density and the short-range interaction. These corrections are estimated as difference between the total charge densities and the short-range interactions for the regular MM and the reference QM structures of the unperturbed lattice, calculated in two preparatory steps 1 and 2, respectively:

$$E_{int}^{corr} = (\rho_{cl}^{tot,MM}(R_{cl}^{reg}, R_{pp}^{reg}) - \rho_{cl}^{tot,QM}(\rho_{cl}^{ref}, R_{cl}^{ref}, R_{pp}^{ref}))||\rho_{lat}(R_{lat}) + V_{short}(R_{cl}^{reg}, R_{pp}^{reg}/R_{lat}) - V_{short}(R_{cl}^{ref}, R_{pp}^{ref}/R_{lat}) \quad (1)$$

Here, R_{cl}, R_{pp}, and R_{lat} collectively refer to atomic positions in the cluster, the boundary region, and the lattice environment, respectively, of the regular (*reg*) and the reference (*ref*) structures. The double bar || represents the classical Coulomb interaction between two charge densities. By construction, the environment is assured to retain its MM equilibrium structure if a cluster representing a regular site is embedded.[17] Steps (i) and (ii) need to be performed only once, before an active region, modified by the presence of any type of the defect, can be described in steps (iii) and (iv). The covEPE computational procedure allows one to carry out a completely variational treatment of the total energy with respect to all degrees of freedom of regions I and II.

At variance with most of the other QM/MM schemes, the covEPE method does not use H atoms to cap dandling bonds of the QM cluster but specially adjusted monovalent oxygen pseudoatoms, O*. The interactions of these pseudoatoms with both the rest of the QM cluster and the MM lattice were modified by short-range interaction terms and partial charges $\Delta q_{pp} = -0.3\ e$ located at the position of the O* nuclei. Different from our previous work,[17] in the present study the coupling via the QM/MM border does not only include two-body O*−Si(MM) terms but also three-body interactions of the types O*−Si(MM)−O(MM) and O*−Si(MM)−O*. These extra terms ensure that the geometry of SiO_4 units at the QM/MM boundary remain closer to an ideal tetrahedral configuration. The parameters of these three-body terms were set equal to those for the O−Si−O interaction in our PDC-based force field[17] ($k_\theta = 0.89844$; $\theta_0 = 109.47°$). The parametrization of the pseudopotential and the additional interaction terms were specific for O* centers bound to Si atoms both of the QM cluster and the MM environment; Al atoms were not admitted as neighbors of O* centers to restrict the number of parameters of the current covEPE scheme, but restrictions result when one constructs QM cluster models of Al-containing zeolites (see below). Further details of the covEPE method and the parametrization can be found in ref 17.

2.2. Calculation of the QM Region. All embedded cluster calculations were carried out with the covEPE scheme as implemented in parallel density functional program ParaGauss.[20,21] To treat the QM part of the systems, we used the gradient-corrected exchange-correlation functional as suggested by Becke (exchange) and Perdew (correlation);[22] all calculations were performed in spin-restricted fashion. We described Kohn−Sham orbitals with the following Gaussian-type basis sets, contracted in generalized fashion: (6s1p) → [4s1p] for H, (9s5p1d) → [5s4p1d] for O, (12s9p2d) → [6s4p2d] for Al and Si.[23] The Hartree contribution of the electron−electron interaction was calculated with an auxiliary Gaussian-type representation of the electronic charge density.[24] The corresponding exponents were constructed by scaling the exponents of the orbital basis; a standard set of p and d polarization exponents was added on each atomic center.[25] The structure of the QM clusters as well as the location of the environmental EPE centers were optimized without imposing any symmetry restriction.

As a measure of the acid strength of a bridging OH groups, we calculated their deprotonation energies (DE) by subtracting the total energy of the relaxed neutral (protonic) form of the zeolite and the relaxed anionic (deprotonated) form.

The analysis of OH vibrational frequencies was carried out on optimized structures. The force constant for the vibrational mode was calculated numerically, using finite differences of analytical energy gradients; we invoked the approximation of one independent harmonic oscillator, i.e., only the O−H internal coordinate was varied during the frequency calculation.

2.3. Force Field for Protonic Forms of Aluminosilicates. When we introduced the covEPE approach, we described a strategy for deriving a PDC-based shell-model force field, and we successfully derived a FF for pure siliceous frameworks.[17] Here, we report the extension of this FF to protonic forms of aluminosilicates based on the same parametrization procedure. The following general expression for the total energy is used for the aluminosilicate version of the PDC-based shell model FF:

$$V = \sum_{i,j}\frac{q_i q_j}{r_{ij}} + \sum_{i,j}[A_{ij}\exp(-r_{ij}/\rho_{ij}) - C_{ij}r_{ij}^{-6}] + \sum_i k_i^{sh}\Delta r_i^2 + \sum_{j=T,O} k_\theta(\theta_{ijk} - \theta_0)^2 \quad (2)$$

The charges q_i, describing the Coulomb interaction, are estimated for optimized gas-phase clusters, invoking the CHELPG procedure[10] as implemented in the software package Gaussian98.[26] PDCs were determined from BP-DF calculations with a TZV(d,p) basis set, using seven model clusters of 2 to 5 T atoms which were terminated by OH groups (Table 1; see also the Supporting Information). In addition to the PDCs of Si, Al, and H, three different PDC values were assigned to O centers, depending on their position in the framework, O_I and O_{II} for Si−O−Si and Al−

Table 1. Potential-Derived Charges (in *e*) for Aluminosilicate Clusters[a] Optimized without Embedding

	potential-derived charges[b]					
cluster	O_I	O_{II}	O_{III}	Si_I	Al_I	H_I
$Si_3O_{10}H_8$ [c]	−0.48			1.20		
$Si_4O_{12}H_8$ [d]	−0.48			1.11		
$AlSiO_7H_7$ [e]			−0.15		1.14	0.35
$AlSi_2O_{10}H_9$ [f]		−0.56	−0.28	1.19	1.13	0.33
$AlSi_2O_{10}H_9$ [g]	−0.43		−0.29	1.14	1.09	0.33
$AlSi_3O_{12}H_9$ [d]	−0.33	−0.47	−0.20	1.07	0.96	0.27
	−0.48					
$AlSi_4O_{16}H_{13}$ [h]		−0.62	−0.34	1.21	1.22	0.35
		−0.67		1.29		
final assignment	−0.6	−0.75	−0.4	1.2	1.1	0.35

[a] For sketches of the model clusters, see Figure 4 in the Supporting Information. [b] For the designation of atom types, see Figure 1. [c] 3T chainlike cluster (Figure 4a). [d] Four-membered ring (Figure 4b,f). [e] 2T model (Figure 4c). [f] 3T Si−Al−Si chainlike cluster (Figure 4d). [g] 3T Al−Si−Si chainlike cluster (Figure 4e). [h] 5T cluster with central Al atom surrounded by O and Si shells (Figure 4g).

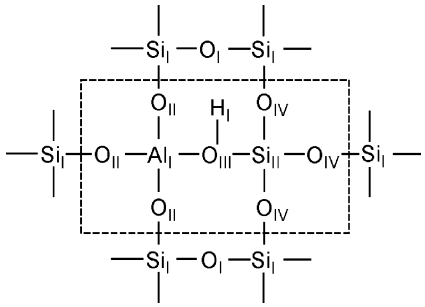

Figure 1. Designation of atomic centers used in the PDC-based shell-model force field for H-zeolites. Centers outside the dashed rectangle are common to the force fields for pure silica and aluminosilicates; centers inside the rectangle are specific to Al-containing lattices.

O−Si bridges, respectively, and O_{III} for a bridging OH group (Table 1 and Figure 1). We took the charges $q(Si_I) = 1.2\ e$ and $q(O_I) = -0.6\ e$ from the FF for pure silica.[17] The other charges, $q(O_{II})$, $q(O_{III})$, $q(Al_I)$, and $q(H_I)$, were restricted by the relation

$$q(Si_I) + 4q(O_I) = q(Al_I) + q(H_I) + 3q(O_{II}) + q(O_{III}) \quad (3)$$

to preserve the neutrality of the zeolite lattice. In other words, the incorporation of Brønsted sites in the framework is assumed to redistribute charge among the centers Al_I, H_I, O_{II}, and O_{III} near the acidic center but leave the charges of the remaining system unchanged (Table 1). Note that the PDC of aluminum, $q(Al_I) = 1.1\ e$, is only 0.1 *e* smaller than that of silicon centers—at variance with the rigid ion force fields of van Santen et al.[13] where the Al charge was fixed to be 1.0 *e* smaller than that of a Si center. Incidentally, our PDC values are similar to the Mulliken charges obtained in a periodic HF calculation of H-chabazite where a small STO-3G basis set had been used:[27] $q(Al) = 1.21\ e$, $q(Si) = 1.42\ e$, $q(O) = -0.71\ e$, $q(H) = 0.21\ e$.

To derive a uniform FF suitable for modeling both siliceous and aluminosiliceous materials, we kept the parameters for stretching (Si_I-O_I, O_I-O_I) and bending interactions ($Si_I-O_I-Si_I$ and $O_I-Si_I-O_I$) as reported earlier for a SiO_2 framework.[17] However, these parameters were found to be unsuitable for describing short-range interactions within a tetrahedron centered on Si in the immediate vicinity of Al−O(H)−Si bridges. To overcome this problem, we defined a further type of oxygen centers, O_{IV}, saturating three of the four bonds of an Si center at an acidic site Al−O(H)−Si; the latter silicon center was reassigned to type Si_{II} (Figure 1). The atomic parameters of Si_{II} and O_{IV} centers (PDCs and core−shell splitting of O_{IV}) were taken from the corresponding centers Si_I and O_I.

Because there is no precise experimental information on the local structure of a zeolite framework in the proximity of Al centers and bridging OH groups, we based the parametrization of the interactions specific to aluminosilica on computational data. For this purpose, we carried out reference QM calculations at the same level as in the subsequent hybrid covEPE calculations, to provide a coherent description of the QM and MM parts of the system. The parametrization procedure consisted of three steps, repeated iteratively until convergence was reached. In the first step, parameters for two-body O−O and O−H interactions [second term in eq 2] and three-body O−T−O interactions [T = Si, Al; fourth term in eq 2] were established, using potential energy curves obtained for the corresponding reference gas-phase cluster from DF calculations (Table 2). Then the pair-potential interactions Si−O and Al−O were determined in the second step. In the third step, the core−shell spring constants, k^{sh}, and the charges of core and shell of polarizable oxygen centers were adjusted to reproduce changes in the dipole moment of the free 3T cluster $(OH)_3Si-O(H)-Al-O-Si(OH)_3$ as induced by point charge of 0.5 *e* located at about 10 Å from the center of the model cluster. Finally, once the values of these iteratively determined parameters had converged, the force constants of three-body interactions, Al−O−Si and H−O−Si(Al), were fitted in a single step. At variance with the Si−O−Si interaction in the silica FF,[17] they were not fitted to experimental data but determined to yield structure and unit cell parameters of H-chabazite. In fact, these results turned out to agree closely with those obtained from the DF-based FF of Sierka and Sauer (Table 3).[16b]

The resulting force field was found to reproduce successfully the structure of isolated acidic sites (also of systems with several such centers) but failed to predict structures where acidic centers are separated by one Si atom only, e.g. where two hydroxyl groups are located in the same 4-ring. Apparently, at a high local Al concentration, oxygen pairs, e.g. $O_{II}-O_{II}$ or $O_{II}-O_{III}$, interact not only via an Al atom but also via a Si center. In such special cases, global short-range parameters determined for all interactions within the common cutoff of 8 Å do not seem to work well. To avoid this problem, we added a local two-body interaction of O−O type to the force field (with a smaller cutoff of 4 Å) which acts only *within* certain tetrahedra; see Table 2. Thus, only pairs of O centers bound to the *same* T atom interact via this additional term.

In Table 4, we provide several examples that demonstrate the performance of our new PDC-based FF for alumino-

Table 2. Parameters[a] of a PDC-Based Shell-Model Force Field for the Protonic Form of Aluminosilicates

	short-range parameters		
FF interaction	*A*, eV	ρ, Å	*C*, eV Å^6
	Two-Body		
Al_I-O_{II} [b]	29617.225	0.189495	122.39
Al_I-O_{III} [b]	40768.575	0.197235	181.04
$Si_I-O_I = Si_I-O_{IV}$	51431.799	0.174872	131.11
Si_I-O_{II} [c]	35091.342	0.190375	174.57
$Si_{II}-O_{II}$	35291.445	0.189265	187.52
$Si_{II}-O_{III}$ [d]	40184.694	0.183955	166.99
$Si_{II}-O_{IV}$ [d]	55400.776	0.172102	144.27
$O_I-O_I = O_I-O_{IV}$	95169.354	0.199100	43.636
O_I-O_{II} [c] $= O_{II}-O_{IV}$	17471.593	0.268175	413.39
$O_{II}-O_{IV}$ (T = Si_{II})[e]	30471.574	0.259285	159.59
$O_I-O_{III} = O_{III}-O_{IV}$ [d]	38115.954	0.239040	125.58
$O_{II}-O_{II}$ [b]	93947.963	0.223816	57.488
$O_{II}-O_{II}$ (T = Si_I or Si_{II})[e]	17471.593	0.268175	413.39
$O_{II}-O_{III}$ [b]	9418.570	0.240302	6.4444
$O_{II}-O_{III}$ (T = Si_{II})[e]	37214.853	0.238941	120.98
$O_{IV}-O_{IV}$ [d]	95169.354	0.199100	43.636
$O_{IV}-O_{IV}$ (T = Si_{II})[e]	59194.280	0.238835	147.22
$O_{III}-H_I$ [b]	7518.521	0.117834	2.0915
FF interaction	k_θ, eV rad^{-1}		θ_0, degree
	Three−Body		
$O_{II}-Al_I-O_{II}$ [b]	0.87410		109.47
$O_{II}-Al_I-O_{III}$ [b]	0.84520		109.47
Om−Si_I−On	0.89844		109.47
$O_{II}(O_{IV})-Si_{II}-O_{II}(O_{IV})$[d]	0.86564		109.47
$O_{II}-Si_{II}-O_{III}$ [d] $= O_{IV}-Si_{II}-O_{III}$	0.87080		109.47
$Si_I-O_I-Si_I = Si_I-O_{IV}-Si_{II}$	5.62		163.4
$Al_I-O_{II}-Si_I$	6.72		162.4
$Al_I-O_{II}-Si_{II}$	6.57		163.4
$Al_I-O_{III}-Si_{II}$	6.44		150.3
$Al_I-O_{III}-H_I$	9.65		129.8
$Si_{II}-O_{III}-H_I$	9.75		141.0
$Si_{II}-O_{IV}-Si_{II}$	6.70		166.2

[a] For the definition, see eq 2; see also Figure 1 for the designation of the atom types. [b] From 5T model $(OH)_3Si-O(H)-Al(OSi(OH)_3)_2-OSi(OH)_3$ with central AlO_4 tetrahedron. [c] From 6T model $(OH)_3Si-O(H)-Al(OH)_2-O-Si(OSi(OH)_3)_3$. [d] From 5T model $(OH)_3Al-O(H)-Si(OSi(OH)3)_2-OSi(OH)_3$ with central SiO_4 tetrahedron. [e] Local interaction, valid only within the tetrahedron centered on atom T (see text).

silicates (PDC in Table 4). We compare the force field results on structural parameters of faujasite (Si/Al = 47, 23, 11) with those for zeolite lattices optimized with other first-principles force fields and free QM reference models. In agreement with the B3LYP-based FF which utilizes formal charges (FC in Table 4),[16b] our force field demonstrates no significant structural changes for isolated acidic sites when the Al loading of a unit cell increases. Bond lengths calculated with both FFs agree within 0.03 Å. Except for $Si_{II}-O_{III}$ bonds, the B3LYP-derived FF gives shorter bond distances; that feature seems to be inherited from the B3LYP approach used to generate set the QM reference data. Compared to the B3LYP-based FF, results from our FF turned out to be less sensitive to the presence of neighboring Al centers; in comparison to isolated sites, bond distances of paired acidic sites changed by 0.025 Å in the B3LYP-based FF, whereas such changes do not exceed 0.004 Å in our FF. As expected, our parametrization fits very well the set of reference structure parameters of isolated QM clusters (Table 4). Al_I-O_{II}, $Si_{II}-O_{III}$, and $O_{III}-H_I$ bond lengths agree perfectly between periodic and QM cluster structures; $Si_{II}-O_{IV}$ and Si_I-O_{II} bond distances are reproduced within 0.02−0.03 Å. The largest discrepancy, 0.04 Å, was obtained for the Al_I-O_{III} bond. Note that $Al_I-O_{III}-Si_{II}$ angles from FF and QM calculations agree within 2° although this interaction was not parametrized on QM data.

Table 3. Comparison of Unit Cell Parameters (Å, deg), Elastic Constants (10^{10} Nm^{-2}), and Bulk Modulus (GPa) of H-Chabazite Calculated with Our PDC-Based (PDC) Force Field and a B3LYP-Derived Force Field Based on Formal Charges (FC)

	chabazite (Si/Al = 11)		chabazite (Si/Al = 5)	
	PDC	FC[a]	PDC	FC[a]
a	9.415	9.438	9.359	9.456
b	9.333	9.458	9.513	9.518
c	9.335	9.386	9.246	9.504
α	93.987	94.776	92.924	95.451
β	94.691	93.951	92.541	93.905
γ	93.766	95.363	95.416	94.932
C_{11}	11.08	9.56	8.01	9.54
C_{12}	5.18	5.13	4.18	5.76
C_{13}	6.17	5.79	2.56	5.71
C_{22}	9.94	8.88	8.60	9.35
C_{23}	4.95	5.41	2.37	5.54
C_{33}	11.65	9.88	6.46	9.25
C_{44}	1.51	1.26	1.47	1.16
C_{55}	1.72	1.10	1.41	1.15
C_{66}	1.55	1.08	1.34	1.08
ϵ_{11}	1.61	2.78	1.69	2.85
ϵ_{33}	1.62	2.92	1.65	2.88
ϵ_{11}^∞	1.53	1.43	1.56	1.43
ϵ_{33}^∞	1.53	1.44	1.56	1.43
bulk modulus	69.94	60.73	43.09	62.53

[a] Reference 16b.

Very recently, EXAFS studies[28] on the surrounding of Al centers in zeolites with FAU and MFI structure provided experimental interatomic Al−O and Al−Si distances as well as O−Al−O angles which are suitable for comparison with our results. In line with these data, our force field predicts an Al−O bond in a Al−O(H)−Si fragment 0.2 Å longer (Al_I-O_{III} in Table 4) than in an Al−O−Si bridge (Al_I-O_{II} in Table 4). Our force field is parametrized to reproduce structural data obtained at the BP level, an approach which has a tendency to overestimate bond lengths. This known trend is reflected by our calculated Al−O bond distances in faujasite which are 0.02−0.04 Å longer than the experimental values determined with EXAFS. Similarly, the average measured Al−Si distance, 3.11,[28] is shorter than the corresponding average of calculated distances, by 0.08 Å (Table 4).

In summary, for the first time, we generated a shell-model force field for H-forms of aluminosilicates. This new FF uses realistic charges for the lattice centers and thus is suitable to create an adequate electrostatic field in the vicinity of hydroxyl acidic sites.[17]

Table 4. Selected Structural Parameters (Distances in Å, Angles in deg) for H-Faujasite with 1, 2, and 4 Al Centers in the Unit Cell (Si/Al = 47, 23, 11) Obtained with Our PDC-Based Force Field (PDC) and a B3LYP-Derived Shell Model Force Field Based on Formal Charges (FC)[a,g]

				Si/Al = 23		
parameter[b]	QM model[c]		Si/Al = 47	isolated	paired	Si/Al = 11
Al_I-O_{III} [d]	1.954	PDC	1.910	1.914	1.905, 1.920	1.913
		FC	1.897	1.902	1.869, 1.875	1.897
$Si_{II}-O_{III}$	1.696	PDC	1.686	1.687	1.687, 1.694	1.686
		FC	1.707	1.707	1.731, 1.732	1.704
$O_{III}-H_I$	0.980	PDC	0.985	0.985	0.984, 0.985	0.985
		FC	0.971	0.971	0.968, 0.969	0.971
Al_I-O_{II} [e]	1.709	PDC	1.706	1.705	1.705, 1.712	1.704
		FC	1.714	1.709	1.722, 1.730	1.717
$Si_{II}-O_{IV}$	1.607	PDC	1.632	1.632	1.630, 1.635	1.631
		FC	1.616	1.616	1.608, 1.615	1.613
Si_I-O_{II}	1.604	PDC	1.628	1.625	1.619, 1.626	1.622
		FC	1.598	1.602	1.594, 1.597	1.601
$\langle Al_I-Si_{II}\rangle$[f]		PDC	3.188	3.192	3.192, 3.189	3.189
$Al_I-O_{III}-Si_{II}$	131.6	PDC	129.3	129.7	129.8	129.5

[a] Reference 16b. [b] For the definition of the types of atoms, see Figure 1. [c] Values used for establishing FF parameters (with the exception of the angle $Al_I-O_{III}-Si_{II}$). [d] Exp. 1.87 ± 0.01 Å in ref 28a; 1.89 ± 0.025 Å in ref 28b. [e] Exp. 1.68 Å in ref 28a; 1.66 Å in ref 28b. [f] Averaged value; exp. 3.11 Å in ref 28a. [g] In all structures, the acidic OH groups were located at O1(H) crystallographic positions. Also shown are QM (DFT-BP) results for the QM ref 5T and 6T cluster models in the gas phase; for the description of the clusters, see the footnotes to Table 2 and the Supporting Information.

2.4. Structures Modeled. The QM/MM systems were constructed so that Al-containing QM clusters (exactly, their protonic form) represent *regular* structures of zeolite lattices, i.e., the Al-containing structures were first optimized at the MM level and the nuclei of the QM cluster were placed at the positions of the corresponding MM centers. Structures with Si/Al = ∞ form an exception: there, Al centers were constructed as defects in a pure silica lattice. We denote QM/MM models with x T-atoms and n Al centers in the QM cluster by **xT-nAl−Oz/N**; z refers to the crystallographic position of the oxygen center of the bridging OH group, and N is the Si/Al ratio in the unit cell. The relative position of the Al centers (in the case of more than one Al atom in a unit cell) was chosen to obey Löwenstein's rule, i.e., Al atoms are separated by at least one Si center. Additional conditions were imposed by the specifics how we treat the QM/MM boundary region in our covEPE scheme. As mentioned in section 2.1, we avoided Al(QM)−O* and O*−Al(MM) bonds in QM/MM calculations because they would have required further short-range parameters and an additional type of O* pseudopotential.

2.4.1. Faujasite. The faujasite structure consists of sodalite cages connected via hexagonal prisms which form so-called supercages.[29] The lattice features four- and six-membered rings as parts of these building blocks and twelve-membered windows between the supercages. The pure silica form of faujasite exhibits only one crystallographic T atom position and four oxygen positions in a unit cell. The primitive unit cell of an Al-free structure contains 144 lattice atoms (48 SiO_2 units). The H-forms of faujasite were constructed by replacing Si atoms with Al and adding a charge compensating proton to one of the four neighboring oxygen centers. Structures with Si/Al ratios of 47, 23, and 11 were modeled by inserting 1, 2, and 4 Al atoms per unit cell, respectively. A structure with infinitely small Al content (1 Al center in the entire lattice, Si/Al = ∞) was modeled by introducing the Al center only at the QM level with the surrounding MM lattice being pure silica.

Brønsted acidic sites were represented by various embedded QM cluster models. The smallest, **5T-1Al−O1/∞** and **5T-1Al−O1/47**, have five tetrahedral (T) atoms in the QM cluster with one central Al atom and an acidic proton attached to an O1 crystallographic position (Figure 2a). With the systems **8T-1Al−O1/N** (N = ∞, 47, 23, 11), we studied how the Al content affects the properties of acidic sites; in these model series, chemically identical QM parts represented two coupled 4-rings with a central Al−O(H)−Si bridge terminated by an $OSiO^*_3$ groups at each T atom of the bridge (Figure 2b). We also used an alternative 8T QM model, **8T(4R)-1Al−O1/23**; there, one 4-ring with two opposite T-atoms terminated by $OSiO^*_3$ moieties was embedded in a framework with Si/Al = 23 (not shown in the figure). A pair of acidic sites, located in one four-membered ring, was described with the models **8T-2Al−O1/23** and **10T-2Al−O1/23** (Figure 2c,d). The cluster models **8T-1Al−O3/47** and **10T-1Al−O3/47** (Figure 2e,f) were used to describe Brønsted acidic sites with hydrogen connected to oxygen in an O3 crystallographic position.

2.4.2. ZSM-5. Zeolite ZSM-5 features an MFI lattice which consists of five- and six-membered rings whose edges constitute 10-membered rings that border the largest cavities. The latter rings form straight channels in [010] direction, perpendicularly intersected by zigzag channels in [100] direction. The Al-free form of ZSM-5 exhibits 12 crystallographic positions for Si atoms and 26 for O atoms. The primitive unit cell of pure silica is orthorhombic and comprises 288 atoms in 96 SiO_2 units. We modeled a ZSM-5 structure with Si/Al = 11, a value typical for this material.[19] This Si/Al ratio corresponds to 8 Al atoms and thus 8 bridging OH groups in a unit cell. The eight Al−O(H)−Si bridges in the initial classical optimization of the structure were located in four T7-O17-T4 positions, three T1-O15-

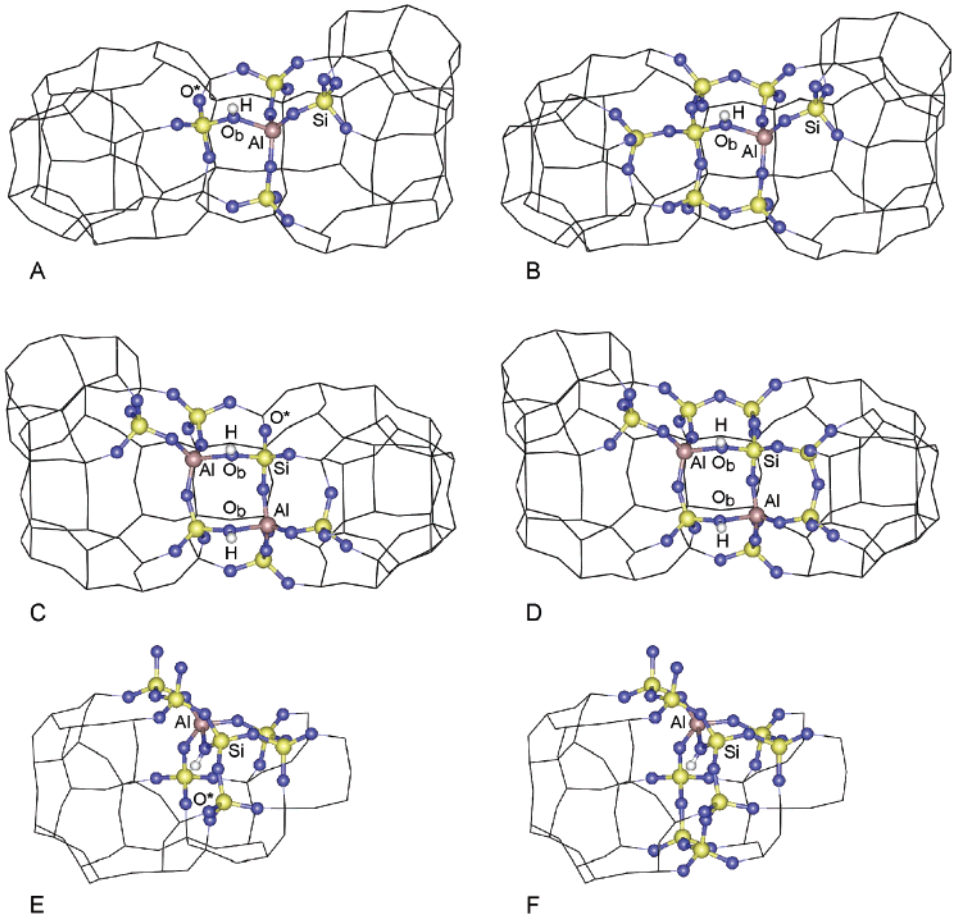

Figure 2. Embedded QM cluster models of various sites of faujasite: a − **5T-1Al**−**O1**, b − **8T-1Al**−**O1**, c − **8T-2Al**−**O1**, d − **10T-2Al**−**O1**, e − **8T-1Al**−**O3**, and f − **10T-1Al**−**O3**.

T10 positions, and one T8-O8-T9 crystallographic positions of the pure silica unit cell. For the QM/MM calculations, we used the cluster model **9T-1Al/11** with a bridging OH group in position O17, e.g. to yield the acidic site Al7−O17(H)−Si4 (Figure 3a) with the OH group directed into a zigzag channel. As experimental information about preferred substitution of T-sites by Al is lacking, we chose the Al positions based on theoretical predictions. In an atomic simulation using an empirical potential, the highest probability for an Al atom in the ZSM-5 lattice was attributed to position T7.[30] Using a DFT-based shell model, Al substitution at T7 was calculated only 5.4 kJ mol^{-1} less stable than the energetically most preferred site T1.[31] The possibility to compare our results with those of the QM-pot cluster embedding approach[32] further motivated us to choose this site.

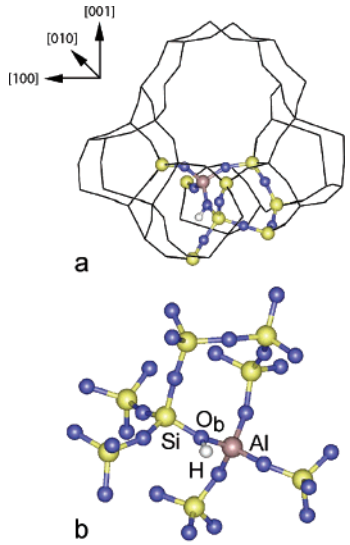

Figure 3. 9T QM model containing the acidic site Al7−O17(H)−Si4 of an HZSM-5 framework: a − view along a straight channel (pseudoatoms O* terminating the QM cluster represented as lines) and b − view from a zigzag channel (surrounding lattice omitted).

3. Results and Discussion

3.1. Effect of QM Cluster Size. Before discussing the framework effects on the characteristics of Brønsted acid sites in QM clusters, we considered computational uncertainties connected with the choice of QM cluster models. With covEPE embedded clusters, a major source of uncertainties could be the QM/MM border and its interaction with the active center (an acidic proton in the present study). The effective Mulliken charge of border oxygen pseudoatoms O* (−0.5 *e*) is less (in absolute value) than the Mulliken charge of real oxygen QM centers[17] (−0.8 *e*), despite the PDC increment of −0.3 *e* assigned to the core of O*. As noted previously,[17] the electrostatic potential close to the O* consequently is 0.02 au more positive than the potential of

Table 5. Selected Structural Parameters (Distances in Å, Angles in deg), Harmonic OH Frequencies ν(OH) (in cm^{-1}), and Deprotonation Energies DE (in kJ mol^{-1}) for Acidic Al−O_b(H)−Si Sites Modeled within QM Clusters Embedded in a Faujasite Lattice of Varying Al Content[l]

Si/Al	∞			47			23				11
cluster	**5T-1Al**[a]	**8T-1Al**[b]	Δ[c]	**5T-1Al**[a]	**8T-1Al**[b]	Δ[c]	**8T-1Al**[b]	**8T-1Al**[d]	**8T-2Al**[d]	**10T-2Al**[e]	**8T-1Al**[b]
Al−O_b	1.954	1.945	−0.009	1.958	1.954	−0.004	1.958	1.949	1.953; 1.923	1.942; 1.916	1.956
Al−O	1.711	1.710	−0.001	1.711	1.712	0.001	1.712	1.706	1.715; 1.700	1.718; 1.701	1.710
Al−O	1.714	1.724	0.010	1.724	1.722	−0.002	1.724	1.723	1.723; 1.719	1.722; 1.724	1.722
Al−O	1.723	1.728	0.005	1.728	1.731	0.003	1.731	1.732	1.739; 1.759	1.739; 1.759	1.733
Si−O_b	1.716	1.718	0.002	1.718	1.722	0.004	1.724	1.717	1.753; 1.742	1.754; 1.742	1.724
O_b-H	0.978	0.978	0.000	0.976	0.978	0.002	0.978	0.978	0.978; 0.976	0.979; 0.976	0.978
H−O*[f]	2.480	4.484		2.618	4.569		4.561	2.751	2.791; 2.773	4.584; 2.756	4.528
H−O_{Al}[g]	2.88	2.62		2.80	2.70		2.72	2.68	2.67; 2.77	2.65; 2.78	2.74
⟨Al−Si⟩[h]	3.19	3.21		3.21	3.21		3.22	3.21	3.21; 3.22	3.21; 3.21	3.21
Al−Al[i]				17.44	17.44		8.65	8.65	4.56	4.56	7.48
O−Al−O_b	98.1;	97.1;		98.1;	99.1;		99.5;	98.8;	99.3; 100.9;	98.9; 104.0;	100.0;
	98.9;	102.;		100.;	102.3;		102.4;	100.4;	108.0/99.9;	107.0/100.7;	102.1;
	101.2	103.9		101.9	102.8		102.8	102.2	101.5; 103.6	101.7; 102.7	102.2
O−Al−O	116.8;	114.4;		116.7;	115.0;		114.4;	115.2;	113.1; 115.8;	112.5; 115.2;	114.6;
	117.6;	115.4;		117.0;	116.0;		115.7;	117.0;	117.0/111.2;	117.0/111.8;	116.2;
	117.8	119.0		117.4	117.6		118.2	118.1	118.3; 118. 5	117.7; 118.5	117.6
Al−O_b−Si	127.5	132.0	4.5	128.7	131.3	2.6	131.3	130.3	127.7; 128.2	128.2; 127.5	131.0
H−O_b−Al	111.3	110.0	−1.3	114.0	111.2	−2.8	111.3	110.3	108.6; 112.1	108.4; 112.7	111.9
H−O_b−Si	112.4	116.3	3.9	117.1	115.8	−1.3	115.6	116.8	116.0; 114.7	114.8; 114.2	115.6
H-opl[k]	8.8	1.8	−7.0	0.2	1.7	1.5	1.8	2.6	7.7; 5.0	8.6; 5.6	1.5
ν(OH)	3747	3714	−33	3754	3720	−34	3721	3730	3727; 3749	3723; 3746	3725
DE	1276	1271	−5	1285	1270	−15	1266	1264	1270	1270	1265

[a] Branched pentameric QM model (Figure 2a). [b] QM cluster in the form of two fused 4-rings (Figure 2b). [c] Changes in parameters of the 8T QM cluster with respect to the 5T QM cluster. [d] QM cluster based on one 4-ring with branches: systems **8T-1Al(4R)**−**O1/23** (not shown) and **8T-2Al**−**O1/23** (Figure 2c). [e] See Figure 2d (DE value for removal of the proton at 4.58 Å from O*). [f] Distance between acidic H and nearest pseudoatom O*. [g] Distance between acidic H and oxygen connected to Al atom. [h] Average Al−Si distance. [i] Shortest distance between Al centers in QM cluster and MM environment. [k] Bending angle of acidic H out of the Al−O_b−Si plane. [l] Bridging oxygen centers O_b of all models are located at O1 crystallographic positions.

a reference MM system comprising an array of potential-derived charges at the lattice positions. Also the Mulliken charge of the Si center close to the border pseudoatom is 0.2 *e* less positive than charge on Si atoms farther from QM/MM border. Therefore, upon embedding of small QM clusters, the electrostatic field in the vicinity of an acidic proton might be perturbed, affecting the properties of the proton. To estimate this effect, we compared results for structure, charge distribution, OH vibrational frequency ν(OH), and deprotonation energy DE when the QM region is extended from a 5T to an 8T cluster model for systems with Si/Al ratio of infinity and 47 (Figure 2a,b).

Comparing calculated structural features of isolated Brønsted sites as obtained with the smaller 5T and the larger 8T QM models, one finds only minor differences in bond lengths (Table 5). The maximum change occurs for the Al−O_b bond: it is about 0.01 Å longer in the smaller models. Other bond distances change at most 0.004 Å. In the 5T models, the H center of the Al−O_b(H)−Si bridge is rather close to terminating pseudoatoms (Figure 2a); thus, bond angles around the O_b center are distorted as compared to the extended 8T QM clusters (Figure 2b), where the acidic site and border centers O* are separated by oxygen and silicon shells. In the 5T model with Si/Al = 47 in the environment, the angle Al−O_b−Si was reduced by 3° and the angle H−O_b−Al increased by 3°. For Si/Al = ∞, larger distortions occur in the 5T model: angles H−O_b−Si and Al−O_b−Si decrease by 4−5° and concomitantly the proton bends 7° more out of the Al−O_b−Si plane. The large perturbations in the latter system may be due to a shorter H−O* distance, 2.48 Å in **5T-1Al**−**O1/**∞ vs 2.62 Å in **5T-1Al**−**O1/47**. The nonbonding distance H−O_{Al} between the proton of the Al−O(H)−Si site and oxygen centers connected to the Al atom is also sensitive to the distance between the active site and the nearest pseudoatom O* (Table 5). Larger H−O* separations in 8T QM models (4.5−4.6 Å vs 2.5−2.6 Å in 5T models) correlate with shorter H−O_{Al} distances, 2.6−2.7 Å, compared to 2.80−2.88 Å in 5T models. Thus, a weaker interaction of H with a pseudoatom O* results in stronger H−O_{Al} interaction. O_{Al} centers are known to exhibit a high basicity;[33] thus, when the interaction of such a center with the acidic proton increases, one expects an elongation of the O−H bond, as is indeed the case (cf. 0.976 Å in **5T-1Al**−**O1/47** vs 0.978 Å in **8T-1Al**−**O1/47**). These deliberations on the proximity of O_{Al} and acidic hydrogen is able to rationalize the difference of the O−H bond lengths in the **8T-2Al**−**O1/23** model; indeed, the OH group at 2.77 from the O_{Al} center is 0.976 Å, while the OH group at 2.67 Å is 0.978 Å (section 3.2).

As a consequence of the above-mentioned structural changes, the charge distribution at the active OH site of small 5T QM clusters differed very slightly from that of larger 8T models. With the larger separation of the active site from border atoms O*, the Mulliken charge of the O_b oxygen

center decreased (by absolute value) from −0.78 to −0.76 *e* and the charge of the proton increased from 0.38 to 0.39 *e*.

In line with the elongation of the O−H bond length by 0.002 Å, the OH vibrational frequency decreases by 33−34 cm^{-1} when the 5T cluster is expanded to an 8T model. The proximity of the QM/MM boundary to the acidic proton also affects the deprotonation energy DE: it decreases by 5−15 kJ mol^{-1} when the size of the QM model increases (Table 5). The QM-Pot embedding scheme also yielded small QM cluster size effects on DE values of faujasite and ZSM-5 lattices, 1−6 kJ mol^{-1}.[9]

The OH frequencies of larger 8T QM clusters are not affected by pseudoatoms, probably because their H−O* distance is larger than in 5T models (see above). This is corroborated by further extending the QM cluster in the 10T models. For instance, in the model **10T-2Al−O1/23** the OH frequency decreases by 4 cm^{-1} (section 3.2) and ν(OH) increases by 6 cm^{-1} (section 3.3). Concomitantly, DE values change at most 12 kJ mol^{-1}. Thus, the features of acidic centers under discussion are already converged for the 8T models.

3.2. Effect of Al Content. In our study we tried to distinguish two ways how the Al content can affect properties of acidic sites in zeolites. First, we considered long-range effects of the overall Al content of the zeolite as monitored by the Si/Al ratio of the MM framework. Second, we studied the direct influence of two Al centers close to each other, by including a second Al center in the QM cluster.

In Table 5 we present the results for QM clusters embedded in a faujasite structure with different Si/Al ratio in the MM region, namely 11, 23, 47, and ∞. As can be seen, the structure of the Al−O_b(H)−Si fragment within the 8T QM cluster is only weakly affected by the Al content of the environment. The Al−O_b and Si−O_b bond lengths involving the protonated oxygen center O_b are elongated only by 0.012 and 0.008 Å, respectively, when the Si/Al ratio decreases from infinity to 11. The other three Al−O bond lengths remain essentially constant; changes do not exceed 0.005 Å. The O_b−H bond distances in the models **8T-1Al−O1/N** with N = 47, 23, 11 are all calculated equal, and only 0.001 Å shorter than for the system **8T-1Al−O1/∞** with a pure-silica environment. Along this series, the average Al−Si distance varies within 0.01 Å only. Pertinent bond angles of all clusters agree within 2°. As the structure of the MM lattice is rather tolerant to changes of the Si/Al ratio from 47 to 11 (Table 4), the MM surrounding imposes very similar steric constraints on all these QM models. This may explain why clusters embedded in the same framework, but with different Al content, yield nearly identical structural parameters. Based on atomistic simulation with the valence force field of Hill and Sauer,[14] faujasite was found to retain its local structure over an even wider range of Si/Al ratios, from 191 to 2.43.

Reduction of the Si/Al ratio in a faujasite lattice from infinity to 11 results in a small increase of the OH vibrational frequency, by 11 cm^{-1} (Table 5), which correlates with minor changes in O−H bond length in this row. Sierka et al. reported[34] a similarly small effect of the chemical composition of the FAU lattice on the O−H stretching frequency in a QM-Pot study. Using 4T embedded QM clusters at the B3LYP level, they determined an increase of the OH frequency by 11 cm^{-1} for the O1(H) position when the Si/Al ratio decreased from 47 to 3; at the HF level, they obtained a positive shift of the same order, 25 cm^{-1}. The calculated trend of increasing frequencies with increasing Al content is in line with experimental observation: for HY zeolite (Si/Al = 20.7 to 2.5), the O1(H) band was found to shift by 17 cm^{-1} to higher frequencies.[35] OH frequencies from fully periodic B3LYP calculations on H-chabazite scattered more.[2] An increase of the Al content from Si/Al = 11 to 3 caused the vibrational frequency of an O1(H) acidic site to increase by 21 cm^{-1}. Even larger Al loading, Si/Al = 1, resulted in a sharp jump of ν(OH) by 24 cm^{-1}. However, this could be an artifact of the computational procedure[2] because in that work zeolite structures (including OH groups) with Si/Al > 1 were optimized at the MM level, at variance with the case Si/Al = 1 where everything was done at the DFT level.

Isolated acidic sites modeled within 8T QM clusters have very similar deprotonation energies, irrespective of the Si/Al ratio in the surrounding MM part. Variations of the DE values, 1265−1271 kJ mol^{-1}, are comparable to the accuracy of the computational modeling; for instance, errors due to the limited size of the QM model are estimated to 5−15 kJ mol^{-1}, see section 3.1. Nearly constant DE values, 1242−1250 kJ mol^{-1} (HF) and 1196−1198 kJ mol^{-1} (B3LYP), were also obtained with 4T QM clusters embedded in FAU environments with Si/Al ratios ranging from 47 to 3.[34]

The present QM/MM study, carried out at the level of mechanical and electrostatic embedding, does not find any strong effect of the Al concentration in the zeolite lattice on structural parameters, spectroscopic features, and deprotonation energies of isolated Brønsted sites. This result can be rationalized by the large spatial separation among pertinent Al−O(H)−Si sites. Indeed, the distance from the Al atom in the QM clusters to the nearest Al center in the surrounding exceeds 7 Å for lattices with the largest Al loading, Si/Al = 11 (Table 5). At such distances, a minor charge redistribution within the MM lattice, induced by incorporating acidic sites (0.1−0.2e for the substitutions $Si_I \rightarrow Al_I$, $O_I \rightarrow O_{II}$, $O_I \rightarrow O_{III}$ and 0.35e for proton addition), is hardly noticeable in the QM region. As corroboration, note that the electrostatic potential in the vicinity of acidic hydrogen centers is perturbed less than 10 kJ mol^{-1} when the Si/Al ratio in the MM environment decreases from 47 to 11.

Al centers in paired acidic sites are only 4.5 Å apart. For such a configuration, **8T-2Al−O1/23** (Figure 2c), the calculated DE value is 6 kJ mol^{-1} higher than for an isolated acidic site, **8T(4R)-1Al−O1/23**: (1270 and 1264 kJ mol^{-1}, respectively; Table 5). We also considered a larger cluster model with two Al centers, **10T-2Al−O1/23**, where, upon removal of an OH group far from the border, we obtained a DE value that was 4 kJ mol^{-1} higher than the corresponding model with one Al center, **8T-1Al−O1/23.** This finding corroborates the assertion that the deprotonation energy grows with the number of Al neighbors of the silicon atom in the Si−O(H)−Al bridge as observed experimentally by

Datka et al.[36] A somewhat larger increase of DE for paired acidic sites was reported in a QM-pot study based on smaller 4T QM cluster models[34] that were embedded in a faujasite lattice; there, the DE values for models with two Al centers were calculated 24−28 kJ mol^{-1} higher for paired 4T-2Al acidic sites compared to isolated 4T-1Al acid sites. A recent DF study based on isolated cluster models of a faujasite 6-ring (containing also two Al centers in next-nearest neighbor positions) also suggested an increase of DE from 1203 kJ/mol for a monoprotonated to 1251 kJ/mol for a diprotonated cluster.[37] Note, however, that our calculations were carried out on larger 8T and 10T QM clusters, at variance with 4T[34] and 6T QM models[37] used in the two studies just mentioned above; also, the present computational approach is more sophisticated.

At variance with deprotonation energies, OH vibrational frequencies were calculated to be sensitive to the presence of an additional Al atom as nearest neighbor of the Si center of the bridging OH group. One OH frequency increased from 3721 cm^{-1} for **8T-1Al−O1/23** to 3749 cm^{-1} for **8T-2Al−O1/23** and to 3746 cm^{-1} for **10T-2Al−O1/23** (Table 5). However, the second OH band (3727 cm^{-1} in **2Al-8T** and 3723 cm^{-1} in **2Al-10T**) remained almost unchanged, exhibiting shifts of only 2−6 cm^{-1} with respect to the frequency of the isolated acidic site. The differentiation of OH frequencies in "paired" acidic sites can be explained by their different crystallographic surroundings. Indeed, the Al center of one Al−O(H)−Si bridge connects to the Si atom of another acidic site via oxygen at an O2 crystallographic position, whereas the Al atom of the other acidic site has an oxygen neighbor at position O3, located in a four-ring with two Al centers. Therefore, the changes due to the close location of two Al−O(H)−Si bridges in the local structures of these acidic sites are different (Table 5). Note that the higher OH frequency corresponds to the OH group with a shorter O−H bond (by 0.002−0.003 Å). Such bond contraction, in turn, weakens the attraction of the proton to the corresponding basic center O_{Al}; cf. the H−O_{Al} distances of 2.77 Å and 2.67 Å for the two sites of **2Al-8T**.

In summary, Al loading of a zeolite lattice affects some of the properties of acidic sites in a noticeable fashion, but only when Al centers are located at closest possible distances, i.e., separated by only one SiO_4 tetrahedron. Such a neighborhood of Al centers results in significant geometry changes of the corresponding acidic sites and a notable increase of the frequency of the nearby OH group. Variation of the Al content far from a bridging OH group does not lead to significant changes in the properties of the active center. A similar conclusion was drawn from an experimental IR study on N_2 sorption at HY samples with Si/Al ratios between 2 and 17.[38]

3.3. Effect of Crystallographic Oxygen Position and Framework Structure. In contrast to the minor influence of the Al loading of the lattice on structure, spectroscopic features, and deprotonation energies of acidic centers, we observed in our modeling that structural constraints of the surrounding framework on the geometry of an Al−O(H)−Si bridge exert a clear effect. In particular, the OH vibrational frequency is sensitive to the crystallographic position of the bridging oxygen center to which the acidic proton is attached. Frequencies corresponding to different crystallographic hydroxyl positions in a faujasite lattice can differ by as much as 85−91 cm^{-1}; see the results for the cluster **8T-1Al−O1/47** modeling an group O1(H) which points inside a 12-membered ring and the clusters **8T-1Al−O3/47** and **10T-1Al−O3/47** modeling O3(H) groups which point inside six-membered rings (Table 6). These results are consistent with the experimentally measured splitting of 73 cm^{-1} between high O1(H) and low-frequency O3(H) bands in IR spectra of faujasites.[35]

Also this frequency difference has a structural origin: the O1−H distance of a hydroxyl group pointing into the larger 12-ring is 0.004 Å shorter than the distance O3−H. This difference may be rationalized by the formation of a weak hydrogen bond across the smaller 6-ring, with oxygen centers at about 2.7 Å from the proton attached to O3. The 12-membered ring is too large for the formation of a hydrogen bond involving the O1(H) group. Because border pseudoatoms O* as a part of the 6-ring of the **8T-1Al−O3/47** model (Figure 2e) are still too close to the active center, they may distort the electrostatic field in the neighborhood of the acidic proton and consequently affect its properties. To exclude this possibility, we included the 6-ring completely in the QM cluster in the **10T-1Al−O3/47** model. Yet, we found the geometrical features and the OH frequency of the 8T and 10T models to be very similar, and we calculate only a very small shift of ν(OH), from 3629 cm^{-1} in the 8T model to 3635 cm^{-1} in the 10T model (Table 6). Therefore, these results demonstrate that the properties under discussion are already converged for the 8T QM cluster and that this model should also be adequate for describing the formation of a H-bond involving the 6-ring.

Despite significant structure and frequency changes, deprotonation energies of O1(H) and O3(H) sites agree within 12 kJ mol^{-1}, using DE values for the **10T-1Al−O3/47** model; this corroborates an earlier finding with QM-Pot modeling.[32,34] The local geometry of an acidic site, its OH vibrational frequency, and energy of proton detachment change drastically with the structure of the framework. The Brønsted site located in the Al7−O17(H)−Si4 position of the HZSM-5 framework (Figure 3) features Al−O_b and Si−O_b bonds that are 0.01−0.02 Å shorter than those of the acidic site O1(H) in faujasite (Table 6). Our results are at variance with structure data of recent EXAFS studies which reported a notably shorter Al−O_b bond, by 0.11 Å, in FAU than in HZSM-5.[28] The deviation in the latter case may be related to the fact that in the experimental sample the OH group is located in a different crystallographic position. However, the discrepancy may also be caused by the limited accuracy of interatomic distances from EXAFS studies as can be seen from the large difference between the experimental values for MFI and FAU, 0.11 Å. Our calculated Al−O_b distances of both types of zeolites, 1.94−1.96 Å, fall between the EXAFS values for FAU and MFI. Moreover, the other calculated Al−O distances not involving the bridging oxygen center O_b (with the proton) have been found almost identical in both materials. Our theoretically predicted shortening of the average Al−Si distance ⟨Al−Si⟩ from 3.21

Table 6. Selected Structural Parameters (Distances in Å, Angles in deg), Harmonic OH Frequencies ν(OH) (in cm^{-1}), and Deprotonation Energies DE (in kJ mol^{-1}) Calculated for Embedded Cluster Models Representing Various Crystallographic Positions of Bridging Oxygen Centers O_b in Faujasite (FAU) and HZSM-5 (Si/Al Ratio Also Shown)

lattice	FAU				HZSM-5	
O(H) site	Al−O1−Si	Al−O3−Si			Al7−O17−Si4	
cluster/Si:Al	**8T-1Al/47**[a]	**8T-1Al/47**[b]	**10T-1Al/47**[c]	exp.	**9T-1Al/11**[d]	exp.[e]
Al−O_b	1.954	1.959	1.955	1.87 ± 0.01,[e] 1.89 ± 0.025 [f]	1.936	1.98 ± 0.01
Al−O	1.712	1.717	1.717	1.68,[e] 1.69[f]	1.721	1.66
Al−O	1.722	1.717	1.718		1.722	1.71
Al−O	1.731	1.718	1.721		1.730	1.74
Si−O_b	1.722	1.725	1.723		1.710	
O_b−H	0.978	0.982	0.982		0.977	
H−O*	4.569	2.763	4.109		3.748	
H−O_{Al}	2.70	2.76	2.78		2.67	
<Al−Si>	3.21	3.23	3.23	3.11[e]	3.17	3.09
$(Al-Si)_{max}$ [g]					3.24	3.28
Al−Al	17.44	17.42	17.42		7.28	
O−Al−O_b	99, 102, 102	99, 102, 102	100, 102, 102		94, 98, 105	97 ± 6
O−Al−O	115, 116, 117	115, 116, 118	114, 115, 119		112, 119, 121	119 ± 6
Al−O_b−Si	131.3	129.3	128.9		125.1	
Al−O−Si	137, 140, 151				128, 143, 150	
H−O_b−Al	111.2	113.4	114.2		109.8	
H−O_b−Si	115.8	117.1	116.6		117.2	
H−opl[h]	1.7	0.2	0.3		7.9	
ν(OH)	3720[i]	3629[j]	3635[j]		3715[k]	
DE	1270	1268	1256		1237	

[a] Figure 2b. [b] Figure 2e. [c] Figure 2f. [d] Figure 3. [e] Reference 28a. [f] Reference 28b. [g] Longest Al−Si distance. [h] Bending angle of acidic H out of the Al−O_b−Si plane. [i] Exp. 3623 cm^{-1}, Si/Al = 20.7, ref 35. [j] Exp. 3550 cm^{-1}, Si/Al = 20.7, ref 35. [k] Exp. 3610−3617 cm^{-1}, Si/Al = 20−13.6; see refs 39 and 40.

Å in FAU to 3.17 Å in HZSM-5 agrees with the experimental observation that the average ⟨Al−Si⟩ contracts from 3.11 (H−FAU, Si/Al = 2.5) to 3.09 Å (HZSM-5, Si/Al = 18).[28a] Likely, the reduction of Al−O−Si bond angles in HZSM-5 contributes in a significant way to this shortening (Table 6); for instance, we calculated the Al−O_b−Si angle in HZSM-5 6° smaller than in H−FAU.

The O_b−H bond in HZSM-5 was determined 0.001 Å shorter, but the OH frequency was calculated at 3715 cm^{-1}, i.e., 5 cm^{-1} lower than for O1(H) in **8T-1Al−O1/47** but 80 cm^{-1} higher than for O3(H) in **10T-1Al−O3/47** (Table 6). This result agrees with IR measurements[39,40] which show the OH band of bridging hydroxyls in HZSM-5 zeolite, 3610−3617 cm^{-1}, only slightly lower than the band of bridging O1(H) groups in high-silica faujasite, 3623 cm^{-1}, but significantly higher than the vibrational frequency of O3(H) sites in faujasite, 3550 cm^{-1}.

The calculated Mulliken charge, 0.39 *e*, of the acidic proton is essentially independent of both the Al content and the position of the OH group; a slightly larger value, 0.40 *e*, was calculated for the cluster O3H cluster due to formation of a weak hydrogen bond.

We calculated the deprotonation of the Al7−O17−Si4 site to proceed easier, DE = 1237 kJ mol^{-1}, compared to the sites O1(H) and O3(H) of a faujasite lattice with DE = 1270 and 1256 kJ mol^{-1}, respectively; see the results for the models **8T-1Al−O1/47** and **10T-1Al−O3/47** (Table 6). The larger energy release accompanying the protonation of HZSM-5 correlates with the stronger distortion of O−Al−O angles in the AlO_4 tetrahedron induced by attaching a proton to one of these oxygen centers.[28a] Indeed, the O−Al−O angles at the Al7−O17(H)−Si4 site of HZSM-5 vary in the range 94−121°, whereas the corresponding angles for an O1(H) site of faujasite vary in a much smaller interval, 99−117° (Table 6). The calculated DE for HZSM-5 is about 10−20 kJ mol^{-1} smaller compared to values calculated previously for four acidic sites in chabazite, 1250−1258 kJ mol^{-1}, using our covEPE scheme.[17] Thus, our covEPE scheme correctly predicts the experimentally observed decrease of the deprotonation energy in the series FAU > CHA > HZSM-5, tentatively estimated from measured shifts of the OH frequency upon adsorption of a probe CO molecule.[41] The lower DE value of HZSM-5 zeolite calculated with our covEPE model is at variance with QM-Pot results[32,42] where the energy for proton removal from site Al7−O17(H)−Si4 in HZSM-5 (Si/Al = 95) was calculated 29−36 kJ mol^{-1} higher than from O1(H) sites in H−Y zeolite (Si/Al = 47). The OM-Pot deprotonation energy of faujasite O1(H) sites remains lower than that of HZSM-5 also for higher Al content (Si/Al = 2.43);[34] even an increase of the number of Al centers near the Si center of an Al−O(H)−Si bridge, which affected the DE values stronger (24 kJ mol^{-1}) than the overall Al content (2−8 kJ mol^{-1}), did not render FAU less acidic than HZSM-5. Thus, in that aspect, QM-Pot results[32,42] did not agree with experiment.[41]

Our comparative study on the effect of two factors—the overall Al content and the structure of the zeolite framework—on OH frequencies and deprotonation energies of Brønsted

centers in FAU and HZSM-5 zeolites shows that the zeolite structure exerts a more pronounced influence on acidic sites. Overall Al loading exerts an effect that is five to six times smaller and hence unable to change the ordering of deprotonation energies between faujasite and HZSM-5.

4. Conclusions

The present study demonstrated that the DFT based covEPE embedding scheme is able to describe aluminosilicate systems. We investigated industrially important zeolites of faujasite and HZSM-5 type. We studied computationally how the Al content affects the local structure, the OH vibrational frequency, and the deprotonation energy of Brønsted acidic sites in zeolite frameworks. For the first time, this problem was considered by fully accounting for both mechanical and electrostatic coupling between QM and MM parts of a hybrid QM/MM system. The newly parametrized shell-model force field for protonic forms of zeolites, assigning potential-derived charges to lattice centers, is an important aspect of the present study. In this way, an adequate electrostatic field[17] is produced in the vicinity of hydroxyl acidic sites in zeolite cavities. We also discussed guidelines for constructing satisfactory QM cluster models that minimize undesirable effects of the QM/MM border region on calculated properties.

Based on the computational results, we concluded that structural features, spectroscopic characteristics, and deprotonation energies of isolated acidic sites in zeolite frameworks with low to medium Al content (Si/Al = 47−11) are similar to those in lattices with infinite Al dilution (Si/Al = ∞). For QM clusters embedded in a faujasite framework with Si/Al ratio from infinity to 11, bond distances and angles change at most by 0.01 Å and 2°, respectively, OH frequencies by 11 cm^{-1}, and deprotonation energies by 6 kJ mol^{-1}. It is crucial to evaluate the effect of the Al content with sufficiently large QM cluster models. Otherwise, computational uncertainties of ∼30 cm^{-1} for OH frequencies and ∼5−15 kJ mol^{-1} for deprotonation energies due to the proximity of the QM/MM border may occur. The influence of *other* Al centers is somewhat more noticeable if their concentration is high enough to generate Al centers at minimum separation from (i.e. as nearest neighbors of) the Si center of the Al−O(H)−Si site. One OH frequency of such "paired" acidic sites is 25−28 cm^{-1} higher than that of an isolated Al−O(H)−Si bridge, whereas the other one remains unchanged within 2−6 cm^{-1}. Observed frequency shifts reflect this nonequivalence of the immediate crystallographic surroundings of the acidic sites which appears when they are close to each other. However, the proton detachment energy is only weakly affected by such structural differences; it was calculated 4−6 kJ mol^{-1} larger than for an isolated OH group.

Effects due to a different local structure of the zeolite framework are larger than those due to changes of the Al content. This stronger influence of the local framework structure was demonstrated for OH frequencies which differ by 85 cm^{-1} between O1(H) and O3(H) sites of a faujasite lattice (Figure 2), although the change in the DE values is rather small, 14 kJ mol^{-1}. With our covEPE embedding strategy, we were also able to reproduce the trend of decreasing proton removal energies (by about 20−25 kJ mol^{-1}) along the series FAU > CHA > HZSM-5, in agreement with experiment. In addition, ordering of and differences between simulated OH frequencies of the three bridging hydroxyl groups, O1(H) (3720 cm^{-1}) and O3(H) (3635 cm^{-1}) of faujasite and the OH group of HZSM-5 (3715 cm^{-1}), very well fit the experimental data: 3623, 3550, 3610−3617 cm^{-1}, respectively.

Acknowledgment. We thank J. D. Gale for providing the latest version of his program GULP. E.A.I.S. gratefully acknowledges an individual grant of the Krasnoyarsk Regional Scientific Foundation (Grant 14G241). This work was supported by Volkswagen-Stiftung (Grant I/73653), INTAS/RFBR (Grant IR-97-1071/RFBR 97-03-71057), Alexander von Humboldt Foundation, Deutsche Forschungsgemeinschaft, Fonds der Chemischen Industrie, and Bulgarian National Science Council.

Supporting Information Available: Sketches of the seven QM clusters used to estimate PDCs, figures of four reference gas-phase QM models utilized for establishing short-range and core−shell parameters of the aluminosilicate force field, table representing core−shell parameters for polarizable oxygen centers, and Cartesian coordinates of all optimized embedded QM clusters. This material is available free of charge via the Internet at http://pubs.acs.org.

References

(1) *Computer Modelling of Microporous Materials*; Catlow C. R. A., van Santen, R. A., Smit. B., Eds.; Academic Press: London, 2004; p 320.

(2) Ugliengo, P.; Civalleri, B.; Zicovich-Wilson, C. M.; Dovesi, R. *Chem. Phys. Lett.* **2000**, *318*, 247−255.

(3) White, J. C.; Hess, A. C. *J. Phys. Chem.* **1993**, *97*, 8703−8706.

(4) Strodel, P.; Neyman, K. M.; Knözinger, H.; Rösch, N. *Chem. Phys. Lett.* **1995**, *240*, 547−552.

(5) Rösch, N.; Vayssilov, G. N.; Neyman, K. M. In *Host−Guest-Systems Based on Nanoporous Crystals*; Laeri, F., Schüth, F., Simon, U., Wark, M., Eds.; Wiley-VCH: Weinheim, 2003; pp 339−357. (b) Rösch, N.; Nasluzov, V. A.; Neyman, K. M.; Pacchioni, G.; Vayssilov, G. N. In *Computational Material Sciences*; Leszczynski, J., Ed.; Theoretical and Computational Chemistry Series, Elsevier: Amsterdam, 2004; Vol. 15, pp 367−438.

(6) Bates, S. P.; van Santen, R. A. *Adv. Catal.* **1998**, *42*, 1−114.

(7) Gonzales, N. O.; Chakraborty, A. K.; Bell, A. T. *Catal. Lett.* **1998**, *50*, 135−139.

(8) Sherwood, P.; de Vries, A. H.; Collins, S. J.; Greatbanks, S. P.; Burton, N. A.; Vincent, M. A.; Hillier, I. H. *Faraday Discuss.* **1997**, *106*, 79−92.

(9) Sauer J.; Sierka, M. *J. Comput. Chem.* **2000**, *21*, 1470−1493.

(10) Chirlian, L. E.; Francl, M. M. *J. Comput. Chem.* **1987**, *8*, 894−905. (b) Breneman, C. M. Wiberg, K. B. *J. Comput. Chem.* **1990**, *11*, 361−373.

(11) Catlow, C. R. A.; Mackrodt, W. C. In *Computer Simulations of Solids, Lecture Notes in Physics*; Catlow, C. R. A., Mackrodt W. C., Eds.; Springer: Berlin, 1982; Vol. 166, p 3.

(12) Blake, N. P.; Weakliem P. C.; Metiu, H. *J. Phys. Chem.* **1998**, *102*, 67−74.

(13) Kramer, G. J.; de Man, A. J. M.; van Santen, R. A. *J. Am. Chem. Soc.* **1991**, *113*, 6435−6441. (b) van Beest, B. W. H.; Kramer, G. J.; van Santen, R. A. *Phys. Rev. Lett.* **1990**, *64*, 1955−1958. (c) Kramer, G. J.; Farragher, N. P.; van Beest, B. W. H.; van Santen, R. A. *Phys. Rev. B* **1991**, *43*, 5068−5080.

(14) Hill, J.-R.; Sauer, J. *J. Phys. Chem.* **1995**, *99*, 9536−9550.

(15) Schröder, K.-P.; Sauer, J.; Leslie, M.; Catlow, C. R. A.; Thomas, J. M. *Chem. Phys. Lett.* **1992**, *188*, 320−325.

(16) Schröder, K.-P.; Sauer, J. *J. Phys. Chem.* **1996**, *100*, 11043−11049. (b) Sierka, M.; Sauer, J. *Faraday Discuss.* **1997**, *106*, 41−62.

(17) Nasluzov, V. A.; Ivanova, E. A.; Shor, A. M.; Vayssilov, G. N.; Birkenheuer, U.; Rösch, N. *J. Phys. Chem. B* **2003**, *107*, 2228−2241.

(18) Czjzek, M.; Jobic, H.; Fitch, A. N.; Vogt, T. *J. Phys. Chem.* **1992**, *96*, 1535−1540.

(19) Barthomeuf D. *Catal. Rev. Sci. Eng.* **1996**, *38*, 521−612.

(20) Belling, T.; Grauschopf, T.; Krüger, S.; Nörtemann, F.; Staufer, M.; Mayer, M.; Nasluzov, V. A.; Birkenheuer, U.; Hu, A.; Matveev, A. V.; Shor, A. M.; Fuchs-Rohr, M. S. K.; Neyman, K. M.; Ganyushin, D. I.; Kerdcharoen, T.; Woiterski, A.; Gordienko, A. B.; Majumder, S.; Rösch, N. ParaGauss version 3.0, Technische Universität München, 2004.

(21) Belling, T.; Grauschopf, T.; Krüger, S.; Mayer, M.; Nörtemann, F.; Staufer, M.; Zenger, C.; Rösch, N. In *High Performance Scientific and Engineering Computing*; Bungartz, H.-J., Durst, F., Zenger, C., Eds.; Lecture Notes in Computational Science and Engineering, Springer: Heidelberg, 1999; Vol. 8, pp 441−455.

(22) Becke, A. D. *Phys. Rev. A* **1988**, *38*, 3098−3100. (b) Perdew, J. P. *Phys. Rev. B* **1986**, *33*, 8822−8824; **1986**, *34*, 7406−7406.

(23) Van Duijneveld, F. B. IBM Res. Report RJ 945, 1971. (b) *Gaussian Basis Sets for Molecular Calculations*; Huzinaga, S., Ed.; Elsevier: Amsterdam, 1984. (c) Veillard, A. *Theor. Chim. Acta* **1968**, *12*, 405−411. (d) Bär, M. R.; Sauer, J. *Chem. Phys. Lett.* **1994**, *226*, 405−412.

(24) Dunlap, B. I.; Rösch, N. *Adv. Quantum Chem.* **1990**, *21*, 317−339.

(25) Chung, S. C.; Krüger, S.; Pacchioni, G.; Rösch, N. *J. Chem. Phys.* **1995**, *102*, 3695−3702.

(26) Frisch, M. J.; Trucks, G. W.; Schlegel, H. B.; Scuseria, G. E.; Robb, M. A.; Cheeseman, J. R.; Zakrzewski, V. G.; Montgomery, J. A., Jr.; Stratmann, R. E.; Burant, J. C.; Dapprich, S.; Millam, J. M.; Daniels, A. D.; Kudin, K. N.; Strain, M. C.; Farkas, O.; Tomasi, J.; Barone, V.; Cossi, M.; Cammi, R.; Mennucci, B.; Pomelli, C.; Adamo, C.; Clifford, S.; Ochterski, J.; Petersson, G. A.; Ayala, P. Y.; Cui, Q.; Morokuma, K.; Malick, D. K.; Rabuck, A. D.; Raghavachari, K.; Foresman, J. B.; Cioslowski, J.; Ortiz, J. V.; Baboul, A. G.; Stefanov, B. B.; Liu, G.; Liashenko, A.; Piskorz, P.; Komaromi, I.; Gomperts, R.; Martin, R. L.; Fox, D. J.; Keith, T.; Al-Laham, M. A.; Peng, C. Y.; Nanayakkara, A.; Gonzalez, C.; Challacombe, M.; Gill, P. M. W.; Johnson, B.; Chen, W.; Wong, M. W.; Andres, J. L.; Gonzalez, C.; Head-Gordon, M.; Replogle, E. S.; Pople, J. A. Gaussian98, Revision A.7, Gaussian, Inc., Pittsburgh, PA, 1998.

(27) Vollmer, J. M.; Stefanovich, E. V.; Truong, T. N. *J. Phys. Chem. B* **1999**, *103*, 9415−9422.

(28) Joyner, R. W.; Smith, A. D.; Stockenhuber, M.; van den Berg, M. W. E. *Phys. Chem. Chem. Phys.* **2004**, *6*, 5435−5439. (b) van Bokhoven, J. A.; van der Eerden, A. M. J.; Prins R. *J. Am. Chem. Soc.* **2004**, *126*, 4506−4507.

(29) http://www.iza-structure.org/databases

(30) Schröder, K.-P.; Sauer, J.; Leslie, M.; Catlow, C. R. A. *Zeolites* **1992**, *12*, 20−23.

(31) Nachtigallova, D.; Nachtigall, P.; Sierka, M.; Sauer, J. *Phys. Chem. Chem. Phys.* **1999**, *1*, 2019−2026.

(32) Eichler, U.; Brändle M.; Sauer, J. *J. Phys. Chem. B* **1997**, *101*, 10035−10050.

(33) Vayssilov, G. N.; Staufer, M.; Belling, T.; Neyman K. M.; Knözinger, H.; Rösch, N. *J. Phys. Chem. B* **1999**, *103*, 7920−7928. (b) Vayssilov, G. N.; Rösch, N. *J. Catal.* **1999**, *186*, 423−432.

(34) Sierka, M.; Eichler, U.; Datka, J.; Sauer, J. *J. Phys. Chem. B* **1998**, *102*, 6397−6404.

(35) Anderson, M. W.; Klinowski, J. *Zeolites* **1986**, *6*, 455.

(36) Datka, J.; Broclawik, E.; Gil, B. *J. Phys. Chem.* **1994**, *98*, 5622−5626. (b) Datka, J.; Gil, B.; Domagala, T.; Gora-Marek, K. *Microporous Mesoporous Mater.* **2001**, *47*, 61−66. (c) Datka, J.; Gil, B.; Baran, P. *J. Mol. Struct.* **2003**, *645*, 45−49.

(37) Vayssilov, G. N.; Rösch, N. *J. Phys. Chem. B* **2001**, *105*, 4277−4284.

(38) Lonyi, F.; Valyin, J.; Pal-Borbely, G. *Microporous Mesoporous Mater.* **2003**, *66*, 272−282.

(39) Zholobenko, V. L.; Kustov, L. M.; Borovkov, V. Yu.; Kazansky, V. B. *Zeolites* **1988**, *8*, 175−178.

(40) Kubelkova, L.; Beran, S.; Lercher, J. A. *Zeolites* **1989**, *9*, 539−543.

(41) Coliccia, S.; Marchese, L.; Martra, G. *Microporous Mesoporous Mater.* **1999**, *30*, 43−56.

(42) Brändle, M.; Sauer, J. *J. Am. Chem. Soc.* **1998**, *120*, 1556−1570.

CT049910N